Journal article published in the Journal of Structural Engineering. The published version may be different from this version

# Seismic Performance of Reinforced Concrete Beams Susceptible to Single-Crack Plastic Hinge Behavior

Eyitayo A Opabola[1*] and Kenneth J Elwood[2]

[1*]Senior Research Fellow, Department of Civil, Environmental and Geomatic Engineering, University College London, London WC1E 6BT, United Kingdom. Email: e.opabola@ucl.ac.uk (corresponding author)

[2]Professor, Department of Civil and Environmental Engineering, University of Auckland, Auckland, 1023, New Zealand. Email: k.elwood@auckland.ac.nz

**Abstract**

Following the 2010/2011 Canterbury and 2016 Kaikoura earthquakes, a number of reinforced concrete (RC) beams in high-rise structures developed a single primary crack at the beam-column interface without the formation of distributed secondary cracks along the beam length. Detailed assessments showed that these beams have conforming longitudinal steel ratios and the single-crack mechanism may be due to design and/or construction practices for beam-column joints in the 1980s. In order to investigate the seismic behaviour of reinforced concrete beams with detailing that inhibited the spread of flexural yielding, an experimental program was carried out on RC beam specimens, having similar reinforcement detailing to that of beams that developed a single crack at their ends during the Kaikoura earthquake to understand their seismic behaviour, post-earthquake reparability, and residual low-cycle fatigue life. Experimental results showed that the beams were able to undergo significant inelastic drift demands without loss of lateral resistance and have sufficient residual drift capacity following moderate and large earthquake demands. The response of the beams specimens was dominated by hinge rotation via bond-slip mechanism. Comparisons showed that the measured drift capacities of the beams exceeded the predicted drift capacities computed using state-of-the-practice procedures.

## Introduction

A major feature in the seismic design of moment-resisting frames is the strong-column-weak beam concept. For a reinforced concrete frame structure to exhibit ductile behaviour during seismic excitations, plastic hinges need to form at the beam ends. Such hinges must have the capability to undergo large inelastic deformations and dissipate energy without tangible strength degradation.

In the last three decades, the inelastic behaviour (especially bond-slip mechanism) of ductile RC beam-column components with conventional distributed cracking mechanism has been studied using experimental and analytical approaches in various studies (Filippou et al. 1983; Saatcioglu et al. 1993; Sezen and Setzler 2008; Tastani and Pantazopoulou 2013). In ductile beams with a conventional distributed cracking mechanism, the contribution of bond-slip mechanism to inelastic deformation is reported to typically range from 15% – 40%. The remaining deformation is due to secondary flexure and flexure-shear cracking along the beam span. Modern concrete design philosophies are hinged on the notion that the response of RC beam-column elements will be dominated by distributed cracking mechanisms. However, following the 2011 Christchurch and 2016 Kaikoura earthquakes, post-earthquake reports (e.g. Smith and Devine (2012)) described the formation of a limited cracking mechanism (and vertical sliding displacement) in beams of modern RC structures (Figure 1).

A huge concern after the 2011 Christchurch and 2016 Kaikoura earthquakes was that the concentrated deformations at the single crack would potentially reduce the plastic rotation capacity of the hinges (it was assumed that strain penetration would occur in only one direction), premature rupture of the reinforcing bars, and lower hysteretic energy dissipation. Also, locally-concentrated strain in the bars may impact the residual low cycle fatigue life available to withstand future earthquakes.

The limited- and single-crack mechanism in RC beams may be attributed to the common construction practice of using cold joints and curtailment of bars close to the column face. Two examples of reinforcement detailing of such beams, found in Wellington buildings, are presented in Figure 2. In precast RC structures, it is not uncommon to find cases where the longitudinal reinforcement in the seating ledge for precast floor units are curtailed at the beam end (Figure 2a) or cases where secondary longitudinal bars provided against shrinkage cracks and/or for proper anchorage of transverse reinforcement are also curtailed at the beam end (Figure 2b & c). According to Choi and Chao (2019), bar curtailment close to the column face is also a common practice in the United States. Hence, a significant number of buildings in the United States may also be susceptible to a single crack plastic hinge response

Figure 3 represents a single-curvature with curtailed bars (similar to Figure 2b and also presented in Figure 4a). As shown in the figure, a lateral load demand *V* corresponding to the yield moment capacity of the beam at section A-A is insufficient to yield the sections adjacent A-A (e.g., B-B). Hence, inelastic deformations starts concentrating at section A-A, leading to a single crack dominated mechanism. For the beam in Figure 3, secondary flexural cracks may develop at sections away from section A-A if the moment demands at these sections is larger than the cracking moment capacity at these sections. As would be discussed subsequently in this paper, the contribution of these secondary cracks to the inelastic behaviour is insignificant compared with the contribution of the single crack at the beam-column interface.

Following the Christchurch Earthquakes, there was concern expressed (See Mander and Rodgers (2015)) that low-cycle fatigue capacity of longitudinal reinforcement in plastic hinge zones may have been significantly reduced as a result of one or more earthquake events in the sequence. It was assumed that the worst-case scenario might be present in components dominated by localised damage mechanisms. This assumption was based on an unproven notion that the localised damage mechanism results in accumulated inelastic strains in the sections of the longitudinal bars at the beam-column interface; hence, quickly consuming the available strain capacity in the bars.

The main aim of the experimental program described in this paper was to investigate the seismic performance of beams with a single-crack plastic hinge. In order to provide a holistic understanding of the response of these components, the experimental program was structured such that the influence of various critical parameters can be studied. Likewise, the reparability and residual deformation capacity of these beams were explored. Furthermore, the adequacy of international seismic assessment guidelines in predicting the response of the test specimens was assessed. While the experimental program focused on beams with curtailed bars, the results presented here may also apply to well-confined conventional RC beams with cold joints.

## Test specimens

### *Beam specimen and test set-up*

As earlier mentioned, RC beams from certain high-rise structures exhibited single-crack plastic hinge response during the 2011 Christchurch and 2016 Kaikoura earthquakes. One such building was a ten-storey RC ductile perimeter frame structure with pre-cast floor units in Wellington designed in 1986 (See Figure 1a for a photo taken from the building). The RC beams of the building had curtailed bar detailing similar to Figure 2b and c. For the sake of confidentiality, this building shall be referred to as Building A in this paper.

Six full-scale RC beam specimens with reinforcement detailing similar to those of actual beams that experienced single-crack plastic hinge behaviour in Building A were constructed. All specimens had cross-sectional dimension of 400mm x 700mm. Also, 10mm transverse stirrups, with spacing of 120mm, were provided in all specimens (Figure 4). Also, the D12 and D16 bars terminate 30mm away from the beam-foundation interface. Figure 5 represents the general test set-up for the beam specimens.

Test specimen details are summarised in Table 1. The description of the specimen ID labels are also provided in Table 1. Four of the beam specimens were nominally identical and had the same reinforcement layout, shear span of 1960mm and an aspect ratio (shear span to effective depth ratio) of 3.2. Specimen CYC-1.24.25 has the same reinforcement layout as the four specimens with a shear span of 1960mm but the shear span was reduced to 1240mm. Specimen CYC-1.24.25 was tested at a shorter aspect ratio to demonstrate the possibility of a change in mechanism to a failure through a diagonal failure plane. It was important to see how these parameters affect the drift capacity of shorter beams expected to have a single-crack plastic hinge response. CYC-1.96.32 had a different reinforcement layout (See Figure 4b), but a similar longitudinal reinforcement ratio. Likewise, the bar grade for the longitudinal reinforcement was different. Specimen CYC-1.96.32 has been detailed to explore the effect of a longer strain penetration length due to the larger bar size and steel grade on the damage mechanism.

All specimens were tested in an upright position (Figure 5). A dynamic actuator with a force capacity of ±300kN and displacement capacity of ±150 mm was used in testing beam specimens CYC-1.24.25, EQ-S-1.96.25, EQ-D-1.96.25 and EQ-R-1.96.25. An actuator with a force capacity of ±1000kN and displacement capacity of ±500 mm was used in testing beam specimen CYC-1.24.25, and CYC-1.96.32 as the expected lateral strength capacity of these two specimens exceeded that of the 300kN actuator.

Global deformations in the specimens and loading frame were measured and monitored throughout the test. A total of 21 instrumentations were used (see Figure 5 and Figure 6). Five displacement gauges were placed on either edge of each specimen to measure axial strains and curvature. Two displacement gauges were connected to the base of the beam and foundation in order to capture fixed-end rotation due to bar slip fully. A displacement gauge and a linear potentiometer were attached to the beam and foundation to provide readings on shear sliding at the base crack (Figure 6). In order to measure shear deformations, two linear potentiometers, arranged in an X-configuration, were adopted. Two vertical string potentiometers were placed on either side of the beam to measure beam elongation. Two in-plane horizontal string potentiometers were used to measure in-plane displacement at the location where beam elongation was measured and at the point of load application. Three LVDTs were also used to check that no form of rocking, horizontal sliding or vertical uplift occurred at the foundation-strong floor interface (note that these LVDTs are not shown in the figures). To avoid influencing the bond-slip response of the longitudinal bars in the test specimens, no strain gauges were attached to the longitudinal reinforcement.

## Loading protocol

### *Specimens CYC-1.96.25, CYC-1.24.25 and CYC-1.96.32*

Three specimens (CYC-1.96.25, CYC-1.24.25 and CYC-1.96.32) were subjected to a standard cyclic protocol at quasi-static rate of 0.75mm/sec (Figure 7). One cyclic reversal to 0.1% and 0.3% drift ratio were followed with two cyclic reversals to 0.6%, 1%, 2%, 3% and so on with increments of 1%.  In each of these three tests, using crack width gauges, crack widths were measured at peak drifts and demand corresponding to zero lateral force (i.e. residual crack width).

### *Specimen EQ-R-1.96.25*

This specimen was used to assess the reparability and low-cycle fatigue performance of a beam with a single-crack plastic hinge. For this procedure, an earthquake-type loading protocol was developed and adopted. The EQ protocol was derived from the displacement history on the ground floor beams extracted from a time history analysis on a 2D model of Building A using a ground motion record at a nearby station from the 2016 Kaikoura Earthquake. Further details on  the model are provided in Opabola (2021).

The adopted initial EQ protocol had a peak drift of 1.03% (Figure 8a). After the initial EQ protocol was concluded, the beam was repaired via epoxy injection by an external contractor and prepared for Part II testing. Details on the repair procedure can be sourced from Opabola (2021)  For Part II, the repaired beam was initially subjected to a peak drift demand which is representative of the building drift under an ultimate limit state (ULS) design level event, computed in accordance with NZS 1170.5 (Standards New Zealand 2004). This ULS drift demand corresponds to 2%. Hence, the ULS design level event was derived by scaling the Part I loading protocol by two. The beam was then subjected to one cycle at peak drift of 3% - corresponding to the drift at which lateral degradation initiated in nominally-identical specimen CYC-1.96.25 (Figure 8a). This allowed for comparison of displacement history effects on the four nominally identical specimens (i.e. CYC-1.96.25, EQ-R-1.96.25, EQ-S-1.96.25 and EQ-D-1.96.25) up until 3% drift. The repaired beam provides information on recoverable stiffness of beams with a single-crack plastic hinge following repair.

After the Part II experiment, the beam was again repaired to test the low-cycle fatigue of a beam that has been through two significant earthquakes (Part III). During Part III experiment, the beam was subjected to a total of 110 cycles at different peak drifts followed by cyclic reversals at large drift demands. Figure 8b provides information on drift demands and number of cycles. Since the intent was to assess the low-cycle fatigue capacity of the reinforcement, it was decided to simulate the axial restraint to beam elongation present in moment-resisting frame buildings. Aside from simulating the restraint to beam elongation, similar to typical low-cycle fatigue tests on bare bars, it was desirable to suppress sliding shear and subject the longitudinal bars to only tension and compression strain reversals. Given that the beam axial force-elongation relationship is building-specific and typically nonlinear, it is difficult to simulate the realistic restraint to beam elongation. A simple elastic axial restraint system, consisting of a spreader beam across the top of the specimen and two 26.5mm high-strength restraining rods, was adopted in this study (See Figure 5b). The elastic restraint system was used to induce an axial compression force linearly proportional to the beam elongation. Prior to testing, the restraining rods were tensioned to provide an initial axial force of 50kN in order to avoid any movement of the spreader beam during testing. This test also provided an opportunity to explore the effectiveness of external post-tensioning system as a practical method of controlling beam-column interface sliding in beams susceptible to single-crack plastic hinge behaviour.

***Specimens EQ-S-1.96.25 and EQ-D-1.96.25***

To explore the influence of displacement rate on seismic response and residual capacity, two specimens, Specimen EQ-S-1.96.25 and EQ-D-1.96.25, were initially subjected to identical displacement histories at a quasi-static and dynamic rate, respectively, followed by a standard cyclic test at quasi-static rate. This procedure has been used in assessing residual capacity of RC bridge piers by Chung et al. (2008). More recently, Marder et al. (2018) adopted the protocol in assessing the residual capacity of conventionally-reinforced ductile RC beams.

The earthquake protocol used for Part I test on EQ-R-1.96.25 was adopted for this purpose. It was, however, scaled to 3% peak drift to match the peak drift from the baseline test (CYC-1.96.25) where onset of bar kinking was first noticed. Following the earthquake protocol, the damaged beam specimens were subjected to the standard loading protocol (Figure 7) at quasi-static rate for both specimens.

### *Material properties*

It is noteworthy that all the specimens were constructed with reinforcing bars and concrete from the same batch, except for Specimen EQ-R-1.96.25 which was built separately. The specified concrete compressive strength was 25MPa and the mean compressive strength obtained from standard compressive strength tests ranged from 26MPa to 31MPa. Three coupon samples of each rebar type were tested to obtain their stress-strain behaviour. Mechanical properties of each type of reinforcing bar are presented in Table 2. As mentioned earlier, Specimen EQ-R-1.96.25 was built separately with a different concrete and reinforcement batch, as designated in Table 2.

## Test observations

Results from the experimental tests are summarised in the following sections. Information provided includes damage pattern and damage progression, force-displacement response, base rotation-displacement demand response, beam elongation response, and base sliding response. These results are used to describe and provide data on the response of beams with a single-crack mechanism.

### *Damage pattern*

*Specimens CYC-1.96.25, CYC-1.24.25, and CYC-1.96.32*

Crack width (residual and peak) measurement and damage progression in Specimens CYC-1.96.25, CYC-1.24.25, and CYC-1.96.32 are presented in Figure 9 and Figure 10. As shown in Figure 10(a-c), the response of CYC-1.96.25 was dominated by damage concentration at the beam end with a number of secondary flexural cracks along the beam span. The widths of the secondary flexural cracks along Specimen CYC-1.96.25 were between 0.1 and 0.25mm throughout the experiment. The response of specimen CYC-1.24.25 was dominated by the concentration of damage at the beam end as well as the initiation and propagation of diagonal cracks along the beam span. In comparison with specimen CYC-1.96-25, more secondary flexural cracks were observed in specimen CYC-1.96.32. These secondary cracks are attributed to the higher yield strength of the longitudinal bars. For specimen CYC-1.96.32, the lateral demand corresponding to the critical section yielding is sufficient to induce flexural cracking along the length of the beam. These secondary cracks were, however, typically less than 0.25mm and did not contribute significantly to the inelastic response of the beam specimen. Furthermore, vertical bond-splitting cracks were observed in CYC-1.96.32. These cracks may also be attributed to the fact that larger dowel mechanism in this specimen resulted in the buckling of the stirrups; thereby, reducing the confinement effect from these stirrups. No bar fracture occurred in any of these tests.

*Specimens EQ-S-1.96.25 and EQ-D-1.96.25*

As previously mentioned, specimens EQ-S-1.96.25 and EQ-D-1.96.25 were both initially subjected to the same loading protocol but at different loading rates. The tests were not stopped during the EQ protocol; hence, the damage state could only be observed at the end of the EQ protocol. The observed damages for both cases were quite similar and the effect of loading rate on damage was not noticeable (Figure 11a and Figure 12a). Also, the damage state was similar to that observed in the Specimen CYC-1.96.25 at 3% drift. The beams were then prepared for the residual capacity test by removing delaminated concrete from the specimens.

For the residual capacity tests, through cycles up to 3%, no additional damage was noticed in both beams. However, more significant shear sliding, in comparison to CYC-1.96.25 was noticeable (Further discussions on shear sliding are presented subsequently). Once the drift demands exceeded 3%, additional concrete spalling initiated due to dowel actions in the longitudinal bars. Similar to other specimens, no bar fracture occurred (Figure 11b & Figure 12b).

*Specimens EQ-R-1.96.25*

Measured residual primary crack width at the base at the end of Part I was 3.6mm with a residual sliding displacement of 1mm. It is noteworthy that post-earthquake evaluation of Building A showed a residual primary crack width of 3 – 4mm and residual vertical sliding displacement of 1.5mm in some of the ground floor beams (See Figure 1a); suggesting that the loading protocol for Part I was sufficient to replicate the real earthquake damage state.

The EQ phase of Part II was run non-stop and visual assessment was only possible at the end of the EQ phase. At the end of the EQ phase, a single crack 6-7mm wide had developed at the base. This crack developed slightly above the previously sealed crack (compare Figure 13a and b). This crack increased to 11-12mm after the final cycle to 3%. Concrete cover spalling occurred at only one edge of the beam specimen (Figure 13b).

The specimen was inspected and epoxy repaired prior to Part III loading. Visual inspection of the main longitudinal reinforcement showed no significant kinking of the bars. As previously mentioned, with the aim of inhibiting a premature sliding shear failure during this experiment, an axial restraint system was employed (Figure 5b). After a total of 110 cycles without a fatigue failure, the beam specimen was loaded monotonically to a drift demand of 8% followed by a pull to -6.5% and eventually a push to 9.5%. The drift demand at the end of the experiment was restricted to the stroke limit of the actuator. During the initial cycles at 1% drift, a single crack was formed at the base of the beam specimen, around the vicinity of the previously sealed crack. Cycles to drift demands of 1.5% and 2% were characterised by the initiation and propagation of cracks from the beam end to a distance of about 130mm along the beam length. Significant spalling of the concrete cover occurred during cycles to drift demand of 2.5% while buckling of the main longitudinal bars only became obvious during cycles to 4% drift. By the end of the experiment at 9.5% drift, the bars had buckled significantly but no bar fracture occurred.

***Force-displacement response***

Load-displacement responses of the beam specimens are presented in Figure 14. The lateral load is the load applied by the actuator while the drift ratio is calculated as the ratio of the displacement demand at the actuator to load height, measured from the beam-foundation interface to the point of lateral load application. From the load-displacement plots, the ultimate drift capacities were measured and presented in Table 3. The ultimate drift capacity was defined as the drift corresponding to 20% loss of lateral resistance. Furthermore, the effective stiffness for all six test specimens, measured using a similar procedure adopted by Opabola and Elwood (2020), are presented in Table 3.

Experimental result show that the baseline specimen, CYC-1.96.25, only suffered lateral failure at 5% drift. A decrease in aspect ratio did not have adverse effect on the cyclic response of the beam as Specimen CYC-1.24.25 also suffered lateral failure at 5%. On the other hand, an ultimate drift capacity of 7% was measured in Specimen CYC-1.96.32.

A comparison of measured peak strength to theoretical flexural strength ($V_{theor}$), computed through a section analysis using measured material properties, show that all components attained their flexural strength (see Figure 14). Specimen EQ-S-1.96.25 reached a peak lateral force of 233.5kN during the quasi-static EQ displacement protocol with a maximum peak drift of 3%. Due to the section loss (See Figure 11a for the damage state of test specimen prior to quasi-static tests) during the EQ protocol, the peak strength of the damaged specimen was only 202kN. Further discussion on the residual performance of these beams is provided subsequently in this paper.

Specimen EQ-R-1.96.25 was able to reach lateral strength of 216kN when pushed to a drift demand of 1%. After repair, when subjected to a peak drift of 3%, the beam reached its full peak strength of 236kN. Expectedly, the repaired beam had suffered no strength degradation at the end of the Part II test.

Contrary to initial assumptions following the 2010/2011 Canterbury and 2016 Kaikoura earthquakes, all the beams in this study were able to undergo significant inelastic deformation without loss of lateral strength. As will be discussed subsequently, the reduction in flexural curvature contribution to the inelastic deformation was compensated for by an increase in bond-slip mechanism contribution.

***Deformation components***

The contribution of various deformation components to the total response of the specimens were extracted from instruments attached to the beams. Interested readers should refer to Opabola (2021) for details on how the deformation components were computed.

Figure 15 shows the contribution of all deformation components to the response of specimens subjected to the standard cyclic protocol (CYC-1.96.25, CYC-1.24.25 and CYC-1.96.32) up to 3% drift demand. To prevent damage, displacement gauges were uninstalled after the cycles to 3% drift were completed. As shown in Figure 15a, prior to yielding of the specimen, bar slip deformation contributes about 48% of the total deformation but this increases to about 80% in the post-yield phase. There is also an increase in shear sliding with increasing drift demands, attributed to axial elongation concentrated at the beam-foundation interface, leading to a reduction in aggregate interlock resistance. Experimental data on the axial elongation-shear sliding behavior of the specimens are available in Opabola (2021). The contributions of deformations due to flexure are also quite prominent during the elastic phase but it fades away with an increase in ductility demands.

Contrary to observations in specimen CYC-1.96.25, CYC-1.24.25 is significantly dominated (about 60%) by bar-slip deformation during the elastic phase. The contribution of bar-slip deformation to the elastic response was about twice the flexural contribution. This is due to the shorter aspect ratio of the beam. Typically, short beam-column components have a larger contribution of bar slip deformation to total yield rotation (Opabola and Elwood 2020). Similar to Specimen CYC-1.96.25, the contribution of bar slip to total deformation during the inelastic phase rises to about 80%. With an increase in drift demand, the contribution of shear sliding at the beam-column interface and shear deformation along the shear span increased.

The elastic response of specimen CYC-1.96.32 is similar to that of CYC-1.96.25. This is not surprising, as studies (Opabola and Elwood 2020) have pointed out that the percentage contribution of different deformation components in the elastic range is not significantly influenced by bar grade or bar size. Likewise, the inelastic responses of specimens CYC-1.96.32 and CYC-1.96.25 up until 3% drift are quite similar.

***Reparability and residual capacity***

Figure 16 compares the hysteresis plot for the baseline specimen (CYC-1.96.25) and the damaged specimens EQ-S-1.96.25 and EQ-D-1.96.25. As shown in Figure 16a, the influence of the initial EQ displacement protocol fades away once the target drift demand exceeds 3% (peak drift of the EQ protocol). The larger strength resistance of the damaged beam in the negative quadrant of the plot is attributed to a lesser amount of 3% cycles in the negative direction. Given the large EQ drift demands on the undamaged EQ-S-1.96.25, one can conclude that, aside from reduced stiffness, unrepaired beams may perform adequately well without reduction in deformation capacity for a subsequent strong earthquake.

Despite similarities in observed damages in Specimens EQ-S-1.96.25 and EQ-D-1.96.25 (see Figure 11a and Figure 12a) at the end of the EQ protocol, a slightly larger reduction in strength was observed in the damaged EQ-D-1.96.25 (Figure 16). It is noteworthy, however, that similar effective stiffness values were measured in both damaged specimens.

As earlier mentioned, the repair of Specimen EQ-R-1.96.25 prior to Part II test only focused on the critical single crack damage zone as it was assumed that in reality, the presence of axial compression would probably make the minor cracks (all less than 0.2mm) away from the interface invisible or practically impossible to inject with epoxy.

During the last few cycles of Part I, the stiffness of the beam had degraded from 0.25 to 0.14$EI_g$. It is noted that the ductility demand at the end of Part I is approximately 2. The initial stiffness of the repaired specimen was 0.165$EI_g$, corresponding to about 17% regained stiffness or 66% of undamaged specimen. This may be due to the fact that only the single crack at the base was repaired and the minor secondary cracks (all less than 0.2mm) may have contributed to lateral deformations. Also, there is a possibility that the epoxy was unable to effectively reinstate the concrete-rebar bond lost due to yield penetration.

Past studies (French et al. 1990; Popov and Bertero 1975; Marder et al. (2018b)) on epoxy repair of RC beams with distributed cracking, subjected to similar or larger level of ductility demand (than Specimen EQ-R-1.96.25) prior to epoxy repair have provided varying results on restored stiffness of repaired specimens. In their test on beam specimens with an aspect ratio of 4.8 subjected to an initial ductility demand of 2, French et al. (1990) observed a 70% reduction in original stiffness during the initial displacement history. Following epoxy injection, the stiffness was restored to 88% of the initial stiffness. Likewise, Marder et al. (2018b) reported that 80-85% of initial stiffness was restored in epoxy-repaired beams (with aspect ratio of 3.8) subjected to initial ductility demands of 4 and 6. On the other hand, Popov and Bertero (1975), noted that only 56% of initial stiffness was regained in an epoxy-repaired beam (aspect ratio of 2.9) subjected to an initial ductility demand of 4.3.

Further examination of the aforementioned experimental programs show that the beams tested by French et al. (1990) and Marder et al. (2018b) have low maximum shear stress values (~ $0.1\sqrt{f'_c}$ in MPa units); hence were flexure-governed. Also, given the aspect ratio of these components, the responses of the beams were dominated mainly by deformation due flexural curvature. On the other hand, the beam tested by Popov and Bertero (1975) was shorter with a high shear stress demand (~ $0.45\sqrt{f'_c}$ in MPa units); hence, the response was dominated by flexure-shear response (i.e. diagonal cracking) with larger contribution of bond-slip deformation.

For flexure-dominated slender beams, bond degradation is lower and the only damage that needs to be repaired are the flexural cracks which are easily reparable; hence the reason for the larger restored stiffness in these cases. For beams dominated by bond-slip deformation, i.e. squat beams and beams with single-crack plastic hinge response, the loss of stiffness during an initial earthquake event is mainly due to concrete-rebar bond degradation. As earlier mentioned, the lower stiffness gain in the repaired components may be attributed to the inability of epoxy to effectively reinstate the concrete-rebar bond lost due to yield penetration.

Hence, in squat beams, beams with high shear stress demand (i.e. $\geq 0.25\sqrt{f'_c}$ in MPa units) and beams with single-crack plastic hinge response, it should be conservatively assumed that only 60% of the initial stiffness can be restored by epoxy injection. It is noteworthy, however, that despite the loss in stiffness, Specimen EQ-R-1.96.25 performed well throughout the Part II test, with no loss in strength (See Figure 14f); suggesting, the strength and deformation capacity of the beam (despite lower stiffness) was not compromised. Additional tests are, however, needed to validate this.

***Low-cycle fatigue test***

To date, low cycle fatigue testing has focused on bar specimens (Kashani et al. 2015; Mander et al. 1994; Tripathi et al. 2018), but very little test data is available on the performance of a complete RC beam plastic hinge. Low cyclic fatigue testing of bar specimens show that tensile fatigue rupture typically occurs after the bar has buckled in the preceding compression cycle (Mander et al. 1994). This implies the plastic strain imposed on the test specimen is a measure of work required to cause sufficient Bauschinger softening to invoke plastic buckling. The plastic strain required to cause rupture of the bar is the cyclic test strain plus the high local curvature strain associated with buckled shape.

El-Bahy et al. (1999) studied the low cycle fatigue characteristics of four nominally identical RC circular columns subjected to cyclic reversals at 2%, 4%, 5.5% and 7%. The authors noted that no significant damage was observed after 150 cycles to 2%. Specimens subjected to 4%, 5.5% and 7% suffered low cycle fatigue failure after 26, 10, 3 cycles, respectively. For the current study, it was of interest to evaluate the effect of accumulated low cycle fatigue damage in a beam, that has been through two significant seismic events up until onset of bar kinking (peak drift of 3%), during future seismic events and aftershock.

The El-Bahy et al. (1999) study is relevant for beam-column components with distributed cracking mechanism. With the aim of studying the low-cycle fatigue behaviour of bond-dominated beams, Erberik and Sucuoglu (2004) tested RC beams with plain longitudinal reinforcement and concluded that the dominating slip mechanism in the beams resulted in a stable hysteresis which is different from what is obtainable in beam-column components with distributed cracking mechanism. Beam specimen EQ-R-1.96.25 provided the interesting opportunity to look at the low-cycle fatigue behaviour of a bond-slip mechanism-dominated beam with deformed bars.

As earlier noted, beam specimen EQ-R-1.96.25 had been axially restrained for Part III in order to suppress sliding shear and subject the longitudinal bars to only tension and compression strain reversals. As shown in Figure 17, after 110 cycles to 2.5%, the low-cycle fatigue test was discontinued and the beam suffered failure in the positive direction at about 9.5% drift. The good performance of the beam is a reflection that contrary to initial assumptions, the low cycle fatigue capacity of longitudinal bars in beams with curtailed bars is not compromised. The low-cycle fatigue response is attributed to the fact that under increased cyclic demands, the longitudinal bars in well-detailed beams susceptible to single-crack plastic hinge behavior, continue to get strained over a longer length (irrespective of the loading protocol). This spread of inelastic deformation in the tensile bars ensures that the strain capacity of the bar is not exhausted; hence the reason no bar fracture was observed in all of the tests. The dominating bond-slip mechanism in beams with a single-crack plastic hinge behaviour may make their low-cycle fatigue response superior to that of beams with distributed cracking. Further testing and analysis are required to validate this. Also, the results of this test suggest that if bar buckling does not occur during an earthquake event, then the moderate yielding sustained will not meaningfully reduce the fatigue life of the reinforcement.

### *Comparison of measured plastic rotation capacity*

*ASCE/SEI 41-17*

Table 10-7 of ASCE/SEI 41-17 provides an estimate for the plastic rotation capacity at lateral failure for flexure-dominated beams as a function of maximum shear stress, longitudinal and transverse reinforcement detailing. The maximum shear stresses ($V_u/(bd\sqrt{f'_c})$) of specimens CYC-1.96.25, CYC-1.96.32 and CYC-1.24.25 are $0.17\sqrt{f'_c}$, $0.22\sqrt{f'_c}$ and $0.26\sqrt{f'_c}$ respectively; hence the predicted plastic rotation at capacity at lateral failure for all three specimens equals 0.025.

Table 4 presents a comparison of measured plastic rotation capacities for CYC-1.96.25, CYC-1.96.32 and CYC-1.24.25 to those predicted using ASCE/SEI 41-17. The measured plastic rotation capacity was computed as the difference between the measured drift capacity (presented in Table 3) and the yield rotation was measured from the force-displacement backbone by drawing a secant line, from the origin to pass through the backbone curve at 70% of maximum lateral load ($V_{max}$), to intersect the horizontal line corresponding to $V_{max}$. Yield rotation is taken as drift at the intersection of the secant line with the horizontal line drawn at $V_{max}$. This approach adapted from Sivaramakrishnan (2010). As shown in Table 4, ASCE/SEI 41-17 underestimates the plastic rotation capacities for all three specimens.

*NZ Guidelines 2017 (MBIE et al. 2017)*

NZ Guidelines (MBIE et al. 2017), published after the 2016 Kaikoura Earthquakes, adopts a moment-curvature approach (Paulay and Priestley 1992) for evaluating the plastic rotation capacity of beams expected to be dominated by single crack plastic hinge response. The guidelines, however, (MBIE et al. 2017) reduced the assumed plastic hinge length by a factor of 0.2. As presented in Paulay and Priestley (1992), the plastic rotation capacity of a beam-column element can be estimated as:

$$\theta_p = \left(\phi_u - \phi_y\right) l_{p,s} \tag{1}$$

Where $\phi_y$ and $\phi_u$ are the yield curvature and ultimate curvature capacity, respectively; $l_{p,s}$ is equivalent single-crack plastic hinge length provided as 20% of the Paulay and Priestley (1992) formulation (Equation (2)).

$$l_{p,s} = 0.2\left(0.08a + 0.022 f_y d_b\right) \tag{2}$$

The ultimate curvature capacity corresponds to the curvature when the maximum concrete compressive strain limit or steel tensile strain limit (as defined by NZ Guidelines (2018)) is attained.

As shown in Table 4, NZ Guidelines (MBIE et al. 2017) underestimates the plastic rotation capacities for all three specimens by a factor of 5. This comparison showed that the reduction factor (i.e. 0.2 times plastic hinge length) adopted by the NZ Guidelines is not appropriate.

*NZ Guidelines 2018 (MBIE et al. 2018)*

Based on the outcome of the current study, the NZ Guidelines provisions for evaluating the plastic rotation capacity of beams expected to be dominated by single crack plastic hinge response was updated to reflect the fact the spread of inelastic deformation is solely through strain penetration. The plastic hinge length equation was updated to:

$$l_{p,s} = (1 + k_{sp}) l_{sp} \tag{3}$$

$l_{sp}$ is the strain penetration length (taken as $0.022 f_y d_b$) and $k_{sp}$ is a factor that reflects the propensity of strain penetration in the longitudinal bars. For beams with curtailed bars such as the beams tested in this paper, $k_{sp}$ is taken to be equal to 1.0. Lower values of $k_{sp}$ are provided in NZ Guidelines 2018 for other single crack conditions (e.g. walls with grout sleeve connectors and drossbach ducts).

As shown in Table 4, NZ Guidelines 2018 (MBIE et al. 2018) provides the best estimate for the plastic rotation capacity of beams with single crack plastic hinge behaviour.

## Conclusions

In comparison with ductile RC beams with significant distributed cracking along the plastic hinge region, the response of modern RC beams expected to exhibit a single-crack plastic hinge behaviour is less understood. Due to a lack of sufficient understanding on the response of components dominated by concentrated deformation at the beam-column interface, these beams are assumed to be susceptible to high tensile strain demands and potential bar fracture under seismic demands.

In order to explore this assumption, the behaviour of six RC beams (five slender and one stocky) susceptible to developing a single-crack plastic hinge was investigated experimentally. Of interest to this study was understanding the seismic behaviour, post-earthquake reparability and residual low-cycle fatigue life of such beams.   The results show that:

- The behaviour of the RC beam specimens was governed by hinge rotation via a bond-slip mechanism at the column face. Bond-slip deformation accounts for up to 80% of total deformation in the beam specimens. In the stocky RC beam specimen, high shear stresses caused the initiation of diagonal cracks along the shear span.  Irrespective of the 'unorthodox' damage mechanisms in the beams, they were able to withstand drift demands larger than 4% without loss in lateral resistance.
- The single crack mechanism did not inhibit the beam from exhibiting desirable ductility. However, as displacement demand increased, the contribution of shear sliding deformation to total deformation increased. Under displacement demands lesser than 2%, shear resistance at the beam-foundation interface is provided through contributions from aggregate interlock and dowel resistance of the longitudinal reinforcement. As displacement increased and the beams elongated, the contribution of aggregate interlock to shear sliding resistance decreased, leading to an increase in shear sliding deformation.

- The residual drift capacity of the earthquake-damaged beams is not highly influenced by previous seismic demands up to 3% drift. There is, however, a reduction in peak strength in unrepaired beams. The reduction in peak strength is attributed to concrete cover delamination or crushing.
- In the repaired specimen in which only the base crack of a damaged beam was repaired, 66% of the stiffness of the undamaged specimen was regained. The low stiffness gain of the repaired beam also suggests that the epoxy may not have effectively reinstated bond lost due to yield penetration. In components susceptible to severe concrete-rebar bond degradation, i.e. beams with high shear stress demand (i.e. $V_u/(bd\sqrt{f'_c}) \geq 0.25\sqrt{f'_c}$ in MPa units) and beams with single-crack plastic hinge response, it should be conservatively assumed that only 60% of the initial stiffness can be restored by epoxy injection. Additional tests are, however, needed to further validate this.
- A low-cycle fatigue test demonstrated the good performance of beams with a single-crack plastic hinge behaviour. This low-cycle fatigue response is attributed to the fact that under increased cyclic demands, the longitudinal bars continues to get strained over a longer length. This spread of inelastic deformation in the tensile bars ensures that the strain capacity of the bar is not exhausted.

**Data Availability Statement**

Some or all data, models, or code that support the findings of this study are available from the corresponding author upon reasonable request (All figures and tables).

**Acknowledgements**

The first author would like to acknowledge the PhD scholarship support from QuakeCoRE – a New Zealand Tertiary Education Commission-funded Centre. This is QuakeCoRE publication number XXX. This experimental program was also supported by QuakeCoRE. The authors would like to acknowledge the advice and assistance provided by Margarita Onishchenko, Matthew Jenkins, Anthony Synge, Tyler Best, Lucas Hogan, Arpit Joshi, Patrick Rogers, Mark Byrami and Nimra Umair during the construction and testing phases of this project.

**References**

Bertero, V. V, and Popov, E. P. (1975). *Hysteretic behavior of ductile moment-resisting reinforced concrete frame components*. College of Engineering, University of California.

Choi, Y., and Chao, S.-H. (2019). “Balanced Damage Concept for Beam-to-Column Connections of Special Moment Frames Using HPFRC.” ACI Structural Journal, American Concrete Institute, 116(1), 237.

Chung, Y., Park, C. K., and Meyer, C. (2008). “Residual Seismic Performance of Reinforced Concrete Bridge Piers After Moderate Earthquakes.” (105), 87–95.

El-Bahy, A., Kunnath, S., Stone, W., and Taylor, A. (1999). “Cumulative seismic damage of circular bridge columns: Variable amplitude tests.” *ACI Structural Journal*, 96(5), 711–719.

Erberik, A., and Sucuogulu, H. (2004). “Seismic energy dissipation in deteriorating systems through low-cycle fatigue.” *Earthquake Engineering & Structural Dynamics*, 33(1), 49–67.

Fenwick, R. C., and Megget, L. M. (1993). “Elongation and load deflection characteristics of reinforced concrete members containing plastic hinges.” *Bulletin of the New Zealand Society for Earthquake Engineering*, 26(1), 28–41.

Filippou, F. C., Popov, E. P., and Bertero, V. V. (1983). *Effects of bond deterioration on* *hysteretic behavior of reinforced concrete joints. Report No NSF/CEE-83032*.

French, C. W., Thorp, G. A., and Tsai, W.-J. (1990). "Epoxy Repair Techniques for Moderate Earthquake Damage." *ACI Structural Journal*, 87(4), 416–424.

Kashani, M. M., Barmi, A. K., and Malinova, V. S. (2015). "Influence of inelastic buckling on low-cycle fatigue degradation of reinforcing bars." *Construction and Building Materials*, Elsevier Ltd, 94, 644–655.

Mander, J. B., Panthaki, F. D., and Kasalanati, A. (1994). "Low-cycle fatigue behavior of reinforcing steel." *Journal of Materials in Civil Engineering*, 6(4), 453–468.

Mander, J. B., and Rodgers, G. W. (2015). "Analysis of low cycle fatigue effects on structures due to the 2010-2011 Canterbury Earthquake Sequence." *Proceedings of the Tenth Pacific Conference on Earthquake Engineering (PCEE)*, Sydney.

Marder, K. J., Motter, C. J., Elwood, K. J., and Clifton, G. C. (2018a). "Effects of variation in loading protocol on the strength and deformation capacity of ductile reinforced concrete beams." *Earthquake Engineering and Structural Dynamics*, 47(11), 2195–2213.

Marder, K., Motter, C., Elwood, K. J., and Clifton, G. C. (2018b). "Testing of 17 identical ductile reinforced concrete beams with various loading protocols and boundary conditions." *Earthquake Spectra*, SAGE Publications Sage UK: London, England, 34(3), 1025–1049.

MBIE, EQC, NZSEE, SESOC, and NZGS. (2017). *Part C5, Concrete buildings, Technical Guidelines for Engineering Assessment Guidelines*. http://www.eq-assess.org.nz/wp-content/uploads/2018/11/c5-concrete-buildings.pdf (Accessed 04 Aug 2021)

MBIE, EQC, NZSEE, SESOC, and NZGS. (2018). *Part C5, Concrete buildings, Technical* *proposal to revise the Engineering Assessment Guidelines*. http://www.eq-assess.org.nz/wp-content/uploads/2018/11/Technical_Proposal_to_Revise_C5_30112018.pdf (Accessed 04 Aug 2021)

Opabola, E. A. (2021). “Seismic Vulnerability Assessment of Existing RC Frame Structures: A Failure mode-based approach.” PhD Thesis. Department of Civil and Environmental Engineering. University of Auckland.

Opabola, E. A., and Elwood, K. J. (2020). “Simplified Approaches for Estimating Yield Rotation of Reinforced Concrete Beam-Column Components.” *ACI Structural Journal*, 117(4), 279–291.

Paulay, T., and Priestley, M. J. N. (1992). *Seismic Design of Reinforced Concrete and Masonry Buildings*.

Popov, E. P., and Bertero, V. V. (1975). “Repaired R/C members under cyclic loading.” *Earthquake Engineering & Structural Dynamics*, 4(2), 129–144.

Saatcioglu, B. M., Alsiwat, J. M., and Ozcebe, G. (1993). “Hysteretic Behavior O F Anchorage Slip in.” 118(9), 2439–2458.

Sezen, H., and Setzler, E. J. (2008). “Reinforcement Slip in Reinforced Concrete Columns.” *ACI Structural Journal*, 105(3), 280–289.

Shah, S. P., Wang, M. L., and Chung, L. (1987). “Model concrete beam-column joints subjected to cyclic loading at two rates.” *Materials and Structures*, 20(2), 85–95.

Sivaramakrishnan, B. (2010). “Non-linear Modeling Parameters for Reinforced Concrete Columns Subjected to Seismic Loads.” Master Thesis. The University of Texas at Austin.

Smith, P. C., and Devine, J. (2012). *Independent assessment on earthquake performance of Craigs investment partners house - 90 Armagh Street. Report prepared for Royal Commission of Inquiry into building failure caused by the Canterbury Earthquakes*. Wellington, NZ.

Standards New Zealand. (2004). *NZS 1170.5 Supp 1:2004 - Structural Design Actions – Part 5 Earthquake Actions – New Zealand*. Wellington, NZ.

Standards New Zealand. (2006). *NZS 3101:2006:A3 - Concrete structures standard.* Wellington, NZ.

Tastani, S. P., and Pantazopoulou, S. J. (2013). "Yield penetration in seismically loaded anchorages: effects on member deformation capacity." Earthq. Struct, 5(5), 527–552.

Tripathi, M., Dhakal, R. P., Dashti, F., and Massone, L. M. (2018). "Low-cycle fatigue behaviour of reinforcing bars including the effect of inelastic buckling." *Construction and Building Materials*, Elsevier Ltd, 190, 1226–1235.

## List of Tables

Table 1 – Test specimens and test matrix

| Specimen ID* | Cross-section type | Aspect ratio ($a/d$) | Bar size $d_b$ (mm) | Steel grade | Test type |
|---|---|---|---|---|---|
| CYC-1.96.25 | A | 3.2 | 25 | 300 | Quasi-static cyclic (0.75mm/s) |
| CYC-1.24.25 | A | 2.0 | 25 | 300 | Quasi-static cyclic (0.75mm/s) |
| CYC-1.96.32 | B | 3.2 | 32 | 500 | Quasi-static cyclic (0.75mm/s) |
| EQ-S-1.96.25 | A | 3.2 | 25 | 300 | Quasi-static EQ (0.75mm/s) + Quasi-static cyclic (0.75mm/s) |
| EQ-D-1.96.25 | A | 3.2 | 25 | 300 | Pseudo-dynamic EQ (75mm/s) + Quasi-static cyclic (0.75mm/s) |
| EQ-R-1.96.25 | A | 3.2 | 25 | 300 | Quasi-static EQ + low-cycle fatigue (0.75mm/s) (Reparability test) |

** - Specimen ID labels is related to the shear span (1.96m or 1.24m), bar size (25mm or 32mm) and loading protocol adopted in the specimens. CYC – Cyclic; EQ – Earthquake protocol; S – Quasi-static; D – Pseudo-dynamic; R - Repaired*

Table 2 – Mechanical properties of transverse and longitudinal reinforcement

| Bar size | Yield stress $f_y$ (MPa) | Yield strain $\varepsilon_y$ | Start of strain hardening $\varepsilon_{sh}$ | Ultimate stress $f_u$ (MPa) | Ultimate strain $\varepsilon_u$ |
|---|---|---|---|---|---|
| 10mm | 326.4 | 0.0026 | 0.018 | 420.7 | 0.2 |
| 12mm | 336 | 0.0018 | 0.026 | 454.6 | 0.22 |
| 12mm* | 316 | 0.0017 | 0.028 | 428 | 0.21 |
| 16mm | 363 | 0.0019 | 0.025 | 535 | 0.2 |
| 16mm* | 315 | 0.0018 | 0.028 | 425 | 0.18 |
| 25mm | 368 | 0.002 | 0.019 | 546.6 | 0.27 |
| 25mm* | 320 | 0.0018 | 0.019 | 466 | 0.21 |
| 32mm | 570 | 0.0029 | 0.017 | 737 | 0.12 |

*Coupon sample from Specimen EQ-R-1.96.25 which was constructed separately

Table 3 – Force-displacement parameters

| Specimen | | $V_{max}$ (kN) | | $V_{max}/(bd\sqrt{f'_c})$ (MPa) | Measured $\theta_y$ (%) | Effective stiffness ($EI_{eff}/EI_g$) | Measured $\theta_u$ (%) |
|---|---|---|---|---|---|---|---|
| | | (+) | (-) | | | | |
| CYC-1.96.25 | | 229.9 | 227.6 | 0.17 | 0.48 | 0.22 | 5.0 |
| CYC-1.24.25 | | 346.4 | 350.7 | 0.26 | 0.4 | 0.16 | 5.0 |
| CYC-1.96.32 | | 299 | 299.3 | 0.22 | 0.8 | 0.2 | 7.0 |
| EQ-S-1.96.25 | EQ | 233.5 | 233.2 | 0.17 | 0.6 | 0.18 | - |
| | CYC | 202 | 202.2 | 0.15 | - | 0.04 | 4.5 |
| EQ-D-1.96.25 | EQ | 248.4 | 250.3 | 0.18 | 0.4 | 0.29 | - |
| | CYC | 186.2 | 189.9 | 0.14 | - | 0.046 | 4.5 |
| EQ-R-1.96.25 | Part I | 203.7 | 216.2 | 0.16 | 0.38 | 0.25 | - |
| | Part II | 229.3 | 236.1 | 0.17 | - | 0.165 | - |

Table 4 - Comparison of measured to predicted plastic rotation capacity

| Specimen | Predicted $\theta_p$ (%) | | | Measured/Predicted | | |
|---|---|---|---|---|---|---|
| | ASCE/SEI 41 (ASCE 2017) | NZ Guidelines (2017) | NZ Guidelines (2018) | ASCE/SEI 41 (ASCE 2017) | NZ Guidelines (2017) | NZ Guidelines (2018) |
| CYC-1.96.25 | 2.5 | 0.8 | 4.0 | 1.8 | 5.5 | 1.1 |
| CYC-1.24.25 | 2.5 | 0.8 | 4.0 | 1.8 | 5.5 | 1.15 |
| CYC-1.96.32 | 2.5 | 1.2 | 6.2 | 2.5 | 5.2 | 1.0 |

**List of Figures**

(a) (b)

Fig. 1 – Single-crack plastic hinge length after the (a) Kaikoura earthquake; (b) Christchurch earthquake (Photos by Synge A and Smith and Devine (2012))

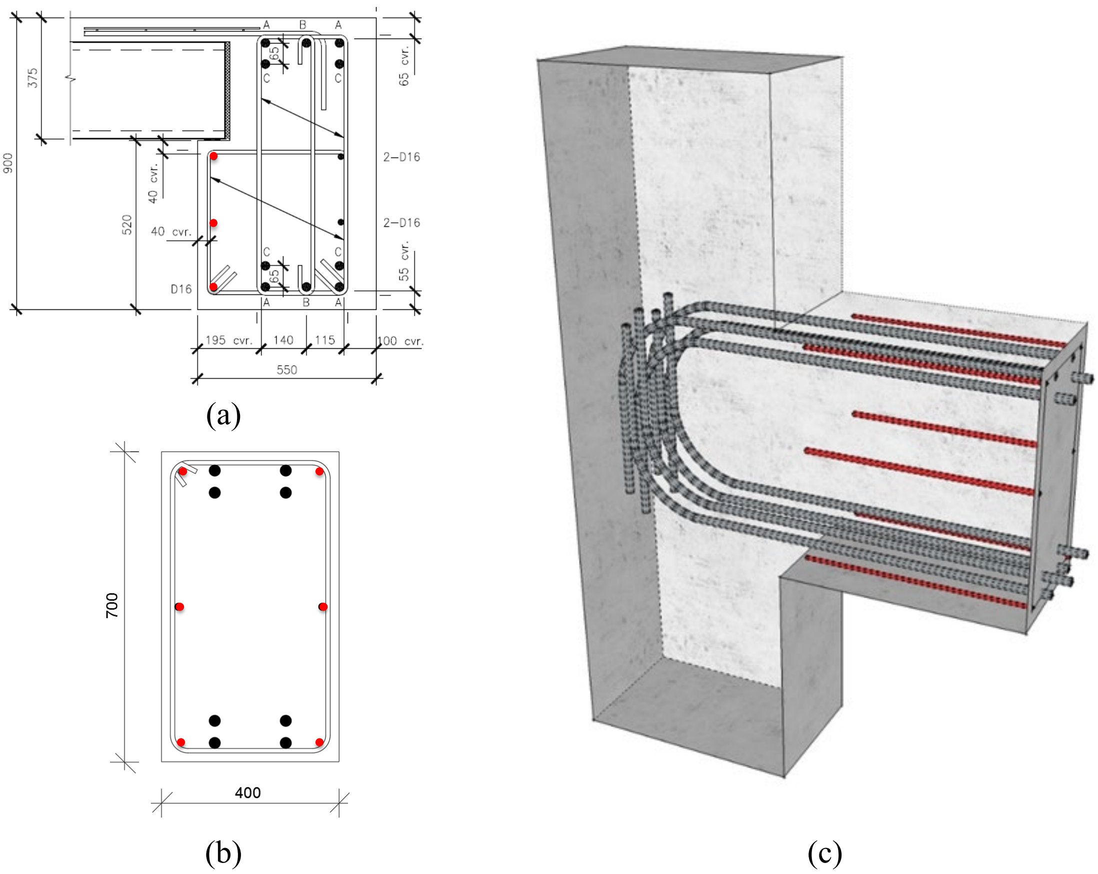


Fig. 2 – Bar curtailment close to the column face. (NB: - Curtailed bars are in red colour in (a), (b) and (c). (c) is a 3D view of (b))

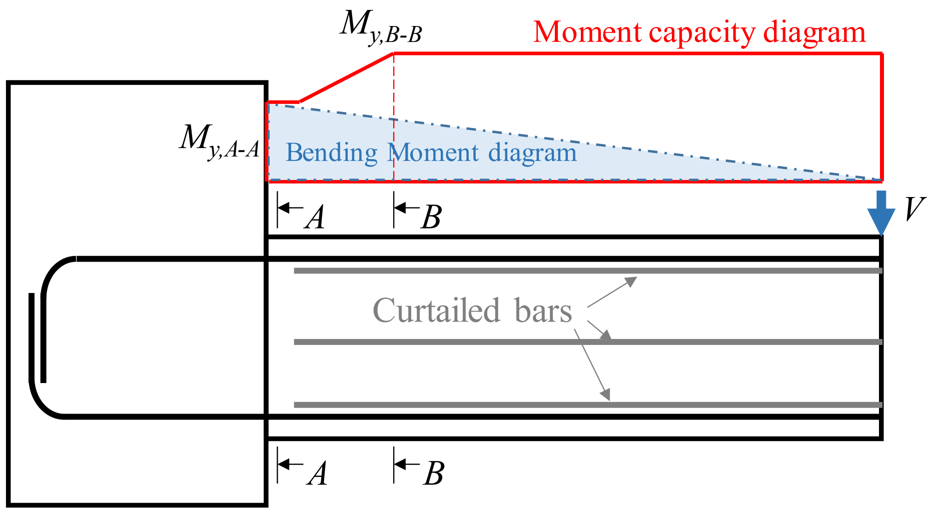


Figure 3 – Graphical explanation for the cause of the single-crack mechanism

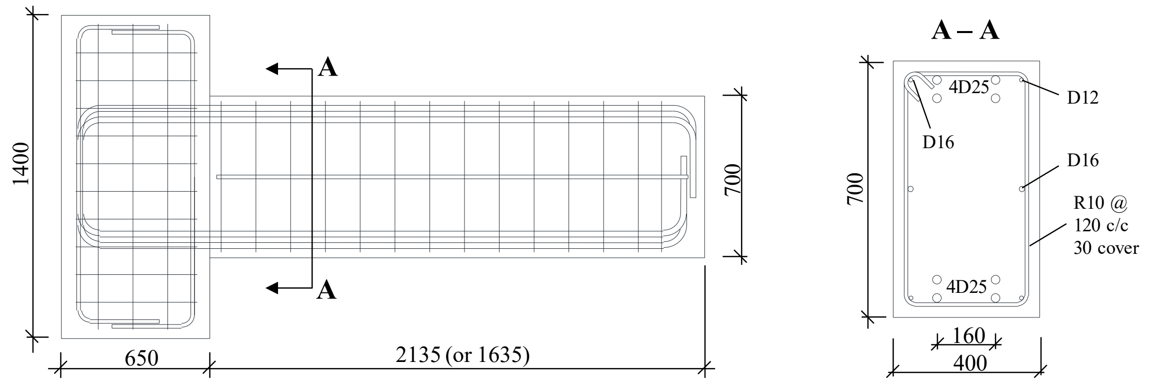


(a) Type A

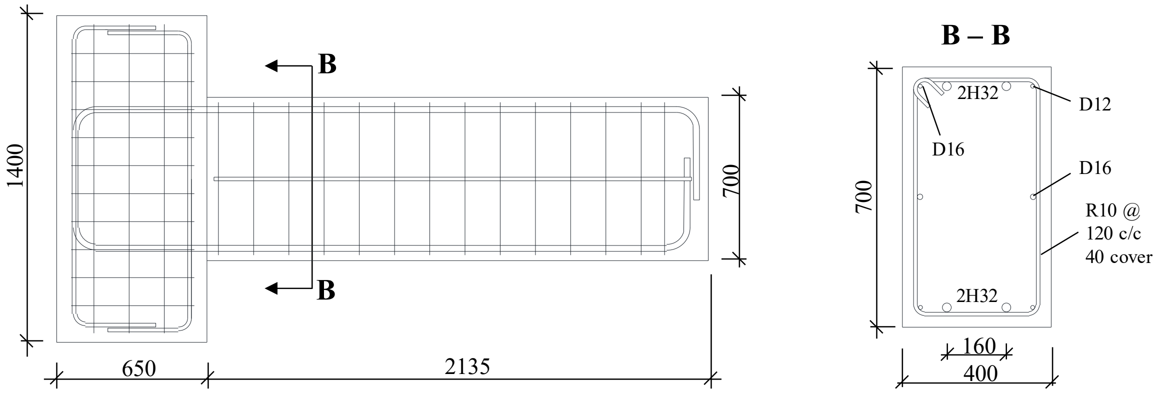


(b) Type B

Fig. 4 – Cross-sectional properties of the beam specimens (NB:- All D12 and D16 bars terminate 30mm away from the beam end. Bars prefixed with R were undeformed Grade 300, bars prefixed with D were deformed Grade 300 and bars prefixed with H were deformed Grade 500E)

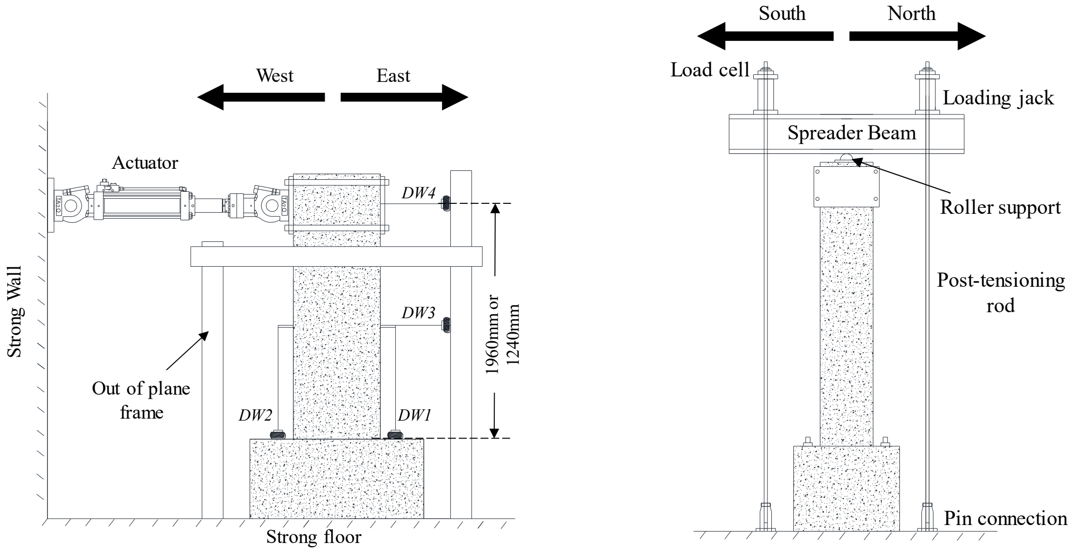


(a) General test set-up showing locations of string potentiometers

(b) Axial restraint system for Specimen EQ-R-1.96.25

Fig. 5 – Details of test set-up

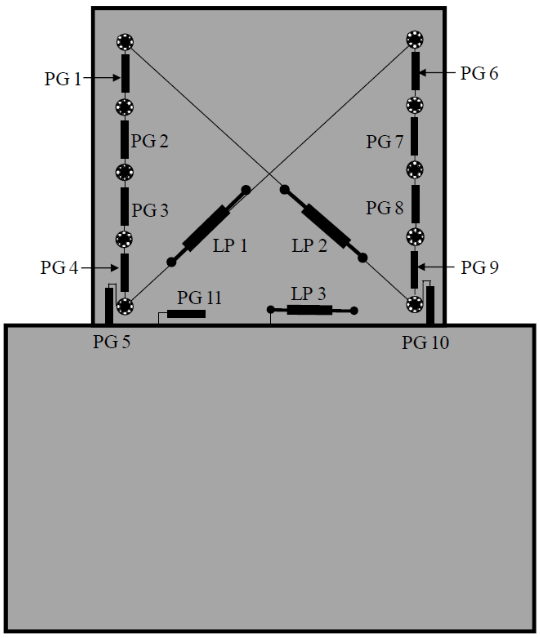


Fig. 6 – Instrumentation layout (The lowest rosettes are 50mm away from the beam end. The vertical distance between other rosettes was 100mm)

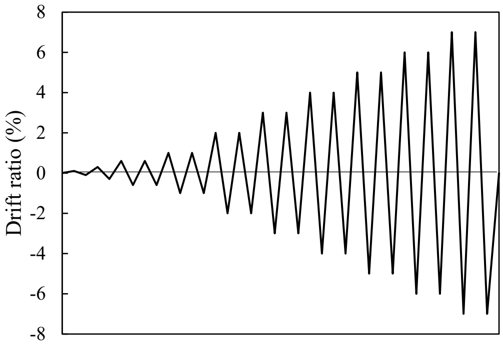


Fig. 7 – Adopted standard cyclic loading protocol

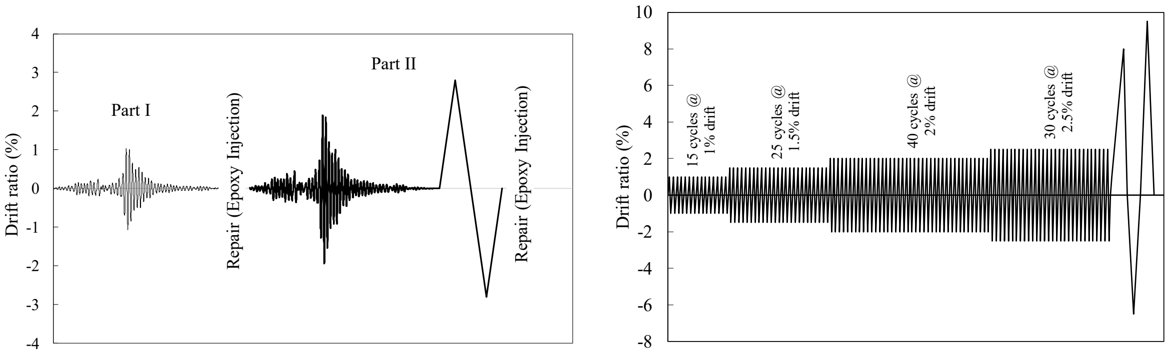


(a) Part I and II

(b) Part III

Fig. 8 – Loading protocol for Specimen EQ-R-1.96.25

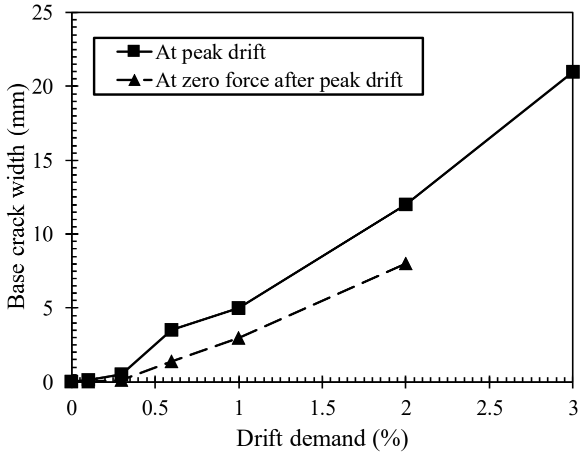


(a) CYC-1.96.25

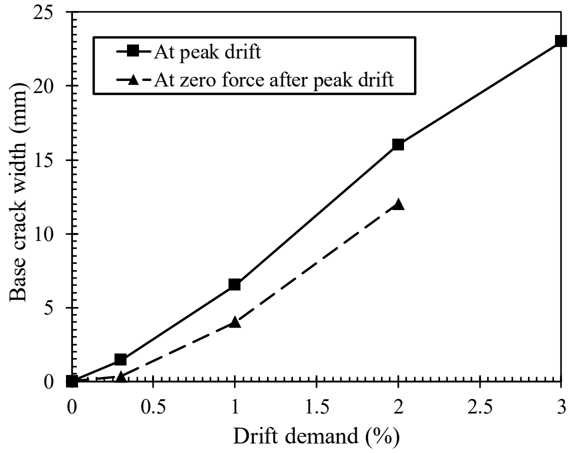


(b) CYC-1.24.25

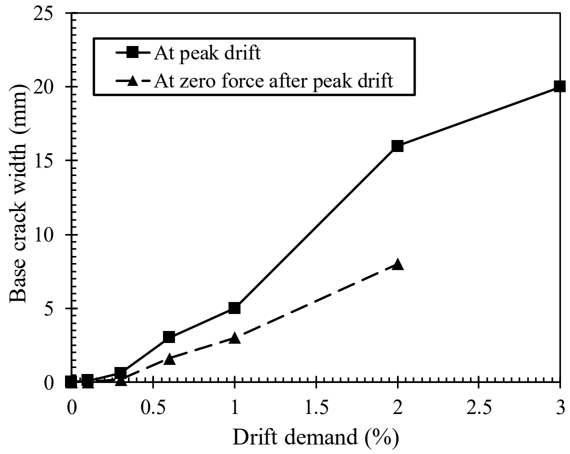


(c) CYC-1.96.32

Fig. 9 – Base crack width at peak drift and residual base crack width at zero force after peak drift in Specimens CYC-1.96.25, CYC-1.24.25 and CYC-1.96.32

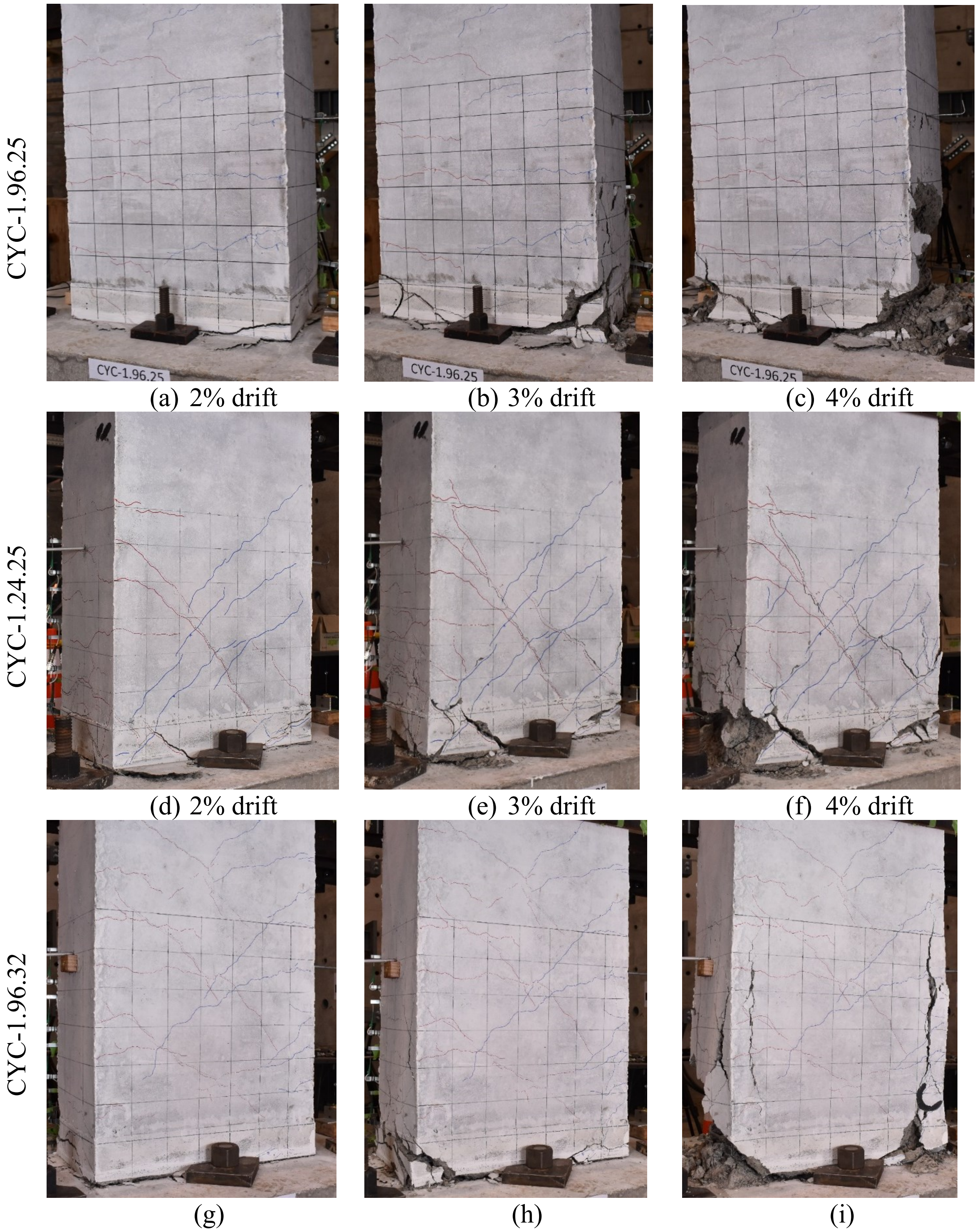


Figure 10 – Damage progression in Specimen CYC-1.96.25, CYC-1.24.25 and CYC-1.96.32

(a) End of EQ protocol

(b) End of Cyclic protocol

Fig. 11 – Pictures of Specimen EQ-S-1.96.25

(a) End of EQ protocol (b) End of Cyclic protocol

Fig. 12 – Pictures of Specimen EQ-D-1.96.25

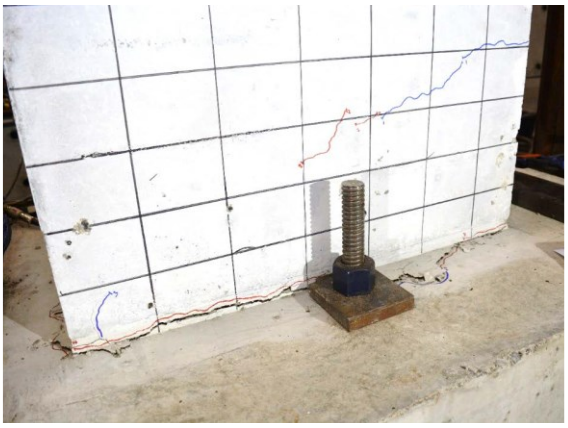

(a) End of Part I

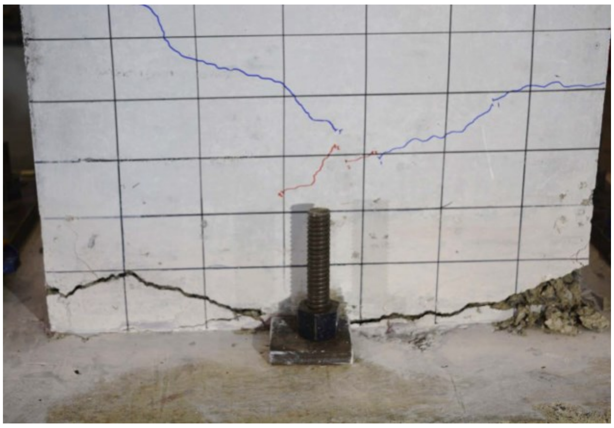

(b) End of EQ phase of Part II

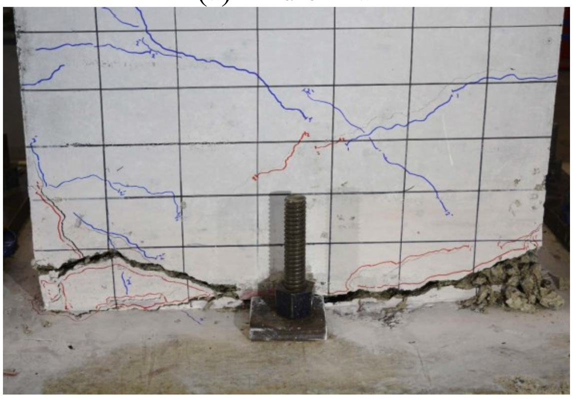

(c) End of Part II full cycle at 3%

(d) After 30 cycles to 2.5% during Part III

Fig. 13 – Photos of Specimen EQ-R-1.96.25

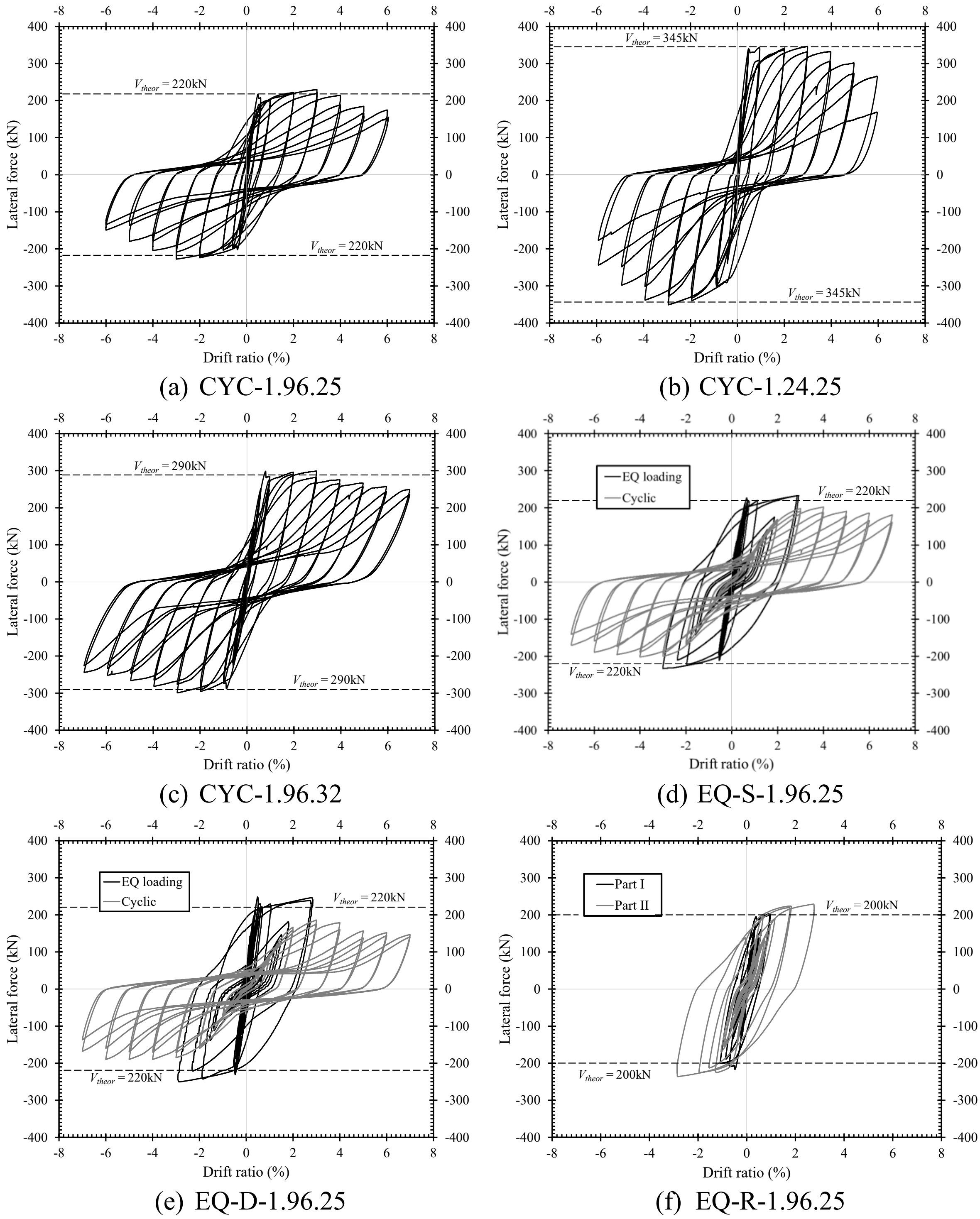


(a) CYC-1.96.25

(b) CYC-1.24.25

(c) CYC-1.96.32

(d) EQ-S-1.96.25

(e) EQ-D-1.96.25

(f) EQ-R-1.96.25

Fig. 14 – Force-displacement response of all beam specimens

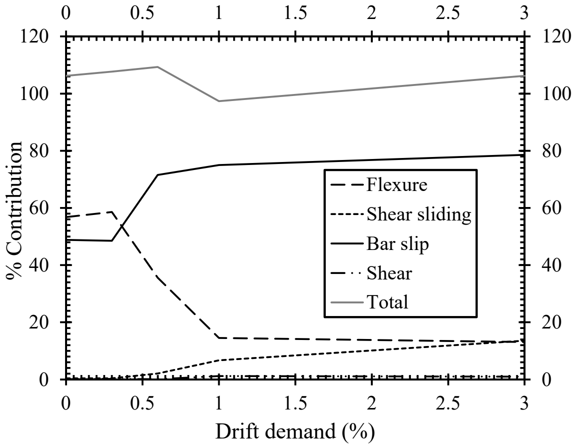


(a) CYC-1.96.25

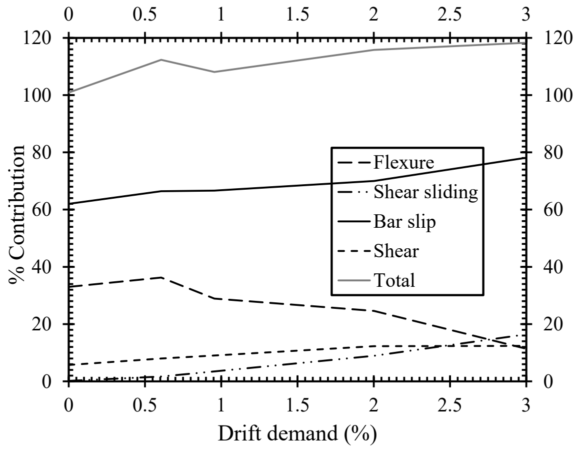


(b) CYC-1.24.25

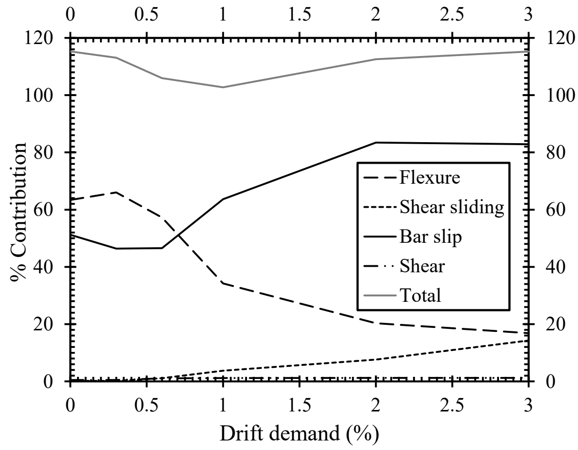


(c) CYC-1.96.32

Fig. 15 – Contribution of deformation components to response of Specimens CYC-1.96.25, CYC-1.24.25 and CYC-1.96.32

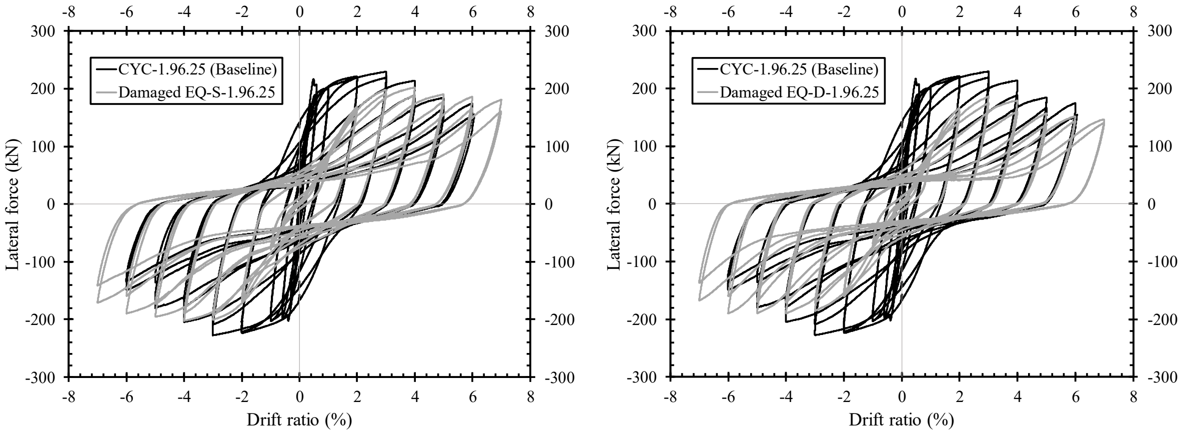


(a) Damaged EQ-S-1.96.25 (b) Damaged EQ-D-1.96.25

Fig. 16 – Residual performance of (a) damaged EQ-S-1.96.25 and (b) EQ-D-1.96.25

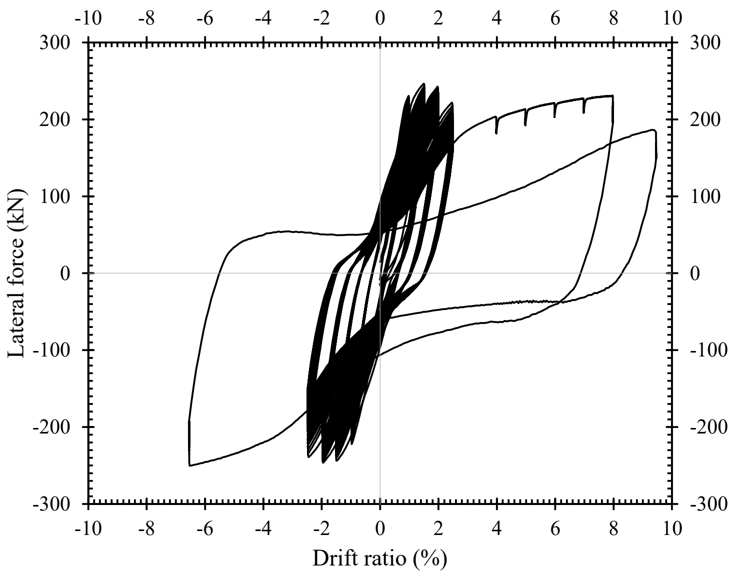


Fig. 17 – Low cycle fatigue test on repaired beam EQ-R-1.96.25.

**List of figure captions**

Figure 1 – Single-crack plastic hinge length after the (a) Kaikoura earthquake; (b) Christchurch earthquake (Photos by Synge A and Smith and Devine (2012))

Fig. 2 – Bar curtailment close to the column face. (NB: - Curtailed bars are in red colour in (a), (b) and (c). (c) is a 3D view of (b))

Fig. 3 – Graphical explanation for the cause of the single-crack mechanism

Fig. 4 – Cross-sectional properties of the beam specimens (NB:- All D12 and D16 bars terminate 30mm away from the beam end. Bars prefixed with R were undeformed Grade 300, bars prefixed with D were deformed Grade 300 and bars prefixed with H were deformed Grade 500E)

Fig. 5 – Details of test set-up

Fig. 6 – Instrumentation layout (The lowest rosettes are 50mm away from the beam end. The vertical distance between other rosettes was 100mm)

Fig. 7 – Adopted standard cyclic loading protocol

Fig. 8 – Loading protocol for specimen EQ-R-1.96.25

Fig. 9 – Base crack width at peak drift and residual base crack width at zero force after peak drift in specimens CYC-1.96.25, CYC-1.24.25 and CYC-1.96.32

Fig. 10 – Damage progression in specimen CYC-1.96.25, CYC-1.24.25 and CYC-1.96.32

Fig. 11 – Pictures of specimen EQ-S-1.96.25

Fig. 12 – Pictures of specimen EQ-D-1.96.25

Fig. 13 – Photos of Specimen EQ-R-1.96.25

Fig. 14 – Force-displacement response of all beam specimens

Fig. 15 – Contribution of deformation components to response of specimens CYC-1.96.25, CYC-1.24.25 and CYC-1.96.32

Fig. 16 – Residual performance of (a) damaged EQ-S-1.96.25 and (b) EQ-D-1.96.25

Fig. 17 – Low cycle fatigue test on repaired beam EQ-R-1.96.25.